JOURNAL OF MATERIALS SCIENCE 33 (1998) 3791–3803

# Polyphenylenesulphide-sealed Ni–Al coatings for protecting steel from corrosion and oxidation in geothermal environments

T. SUGAMA
*Energy Efficiency and Conservation Division, Department of Applied Science. Brookhaven National Laboratory, Upton, NY 11973, USA*
*E-mail: sugama@bnl.gov*

Polyphenylenesulphide (PPS) polymer was applied as a sealing material to flame-sprayed nickel–aluminium (Ni–Al) coatings to protect the interior surfaces at the ends where the mild carbon steel (MCS) heat-exchanger tubes are jointed to the tubesheet. The aim of applying PPS is to prevent their corrosion, oxidation and abrasive wear, in a low pH, hypersaline brine geothermal environment at 200 °C under a hydrothermal pressure of 1.6 MPa. Although the Ni–Al coatings had an excellent thermal conductivity and a good wear-resistance, the inherent open structure of these coatings allowed the hot brine to permeate them easily under such pressure, causing the development of corrosion-induced stress cracks in the MCS. Furthermore, under these conditions, the coatings underwent oxidation with the formulation of $Al_2O_3$ as the major scale compound and NiO as the minor one. PPS sealant was used to solve these problems. However, one major drawback of PPS was its susceptibility to oxidation reaction with hot brine. This reaction not only incorporated more oxygen into the PPS, generating a sulphide → sulphone transformation within PPS, but also it caused the decomposition of PPS, yielding polychloroaryl compound, and sodium sulphate, and also evolving $SO_2$ gases. The $SO_2$ gases had a chemical affinity for oxide scales in Ni–Al, forming water-soluble $Al_2(SO_4)_3$ and $NiSO_4$ salt reaction products at the PPS/Ni–Al interfaces. Despite the occurrence of such oxidation damage in PPS, an exposure for 14 days showed that there was no development of corrosion-caused cracks at the interfaces between the underlying steel and Ni–Al, nor was a striking oxidation of the sealed coating panels.


## 1. Introduction

The key to the successful use of mild carbon steel (MCS) heat-exchanger tubes in a low-pH hypersaline brine geothermal environment at temperatures up to 200 °C, is how to mitigate corrosion and oxidation damage to the interior surfaces of the MCS, and how to design corrosion-preventing barrier layers with a heat-transferable property and hydrothermal stability. An additional problem is how to fabricate a uniform, continuous lining to the interior surface of the tubes, 25 mm inside diameter × 6100 mm long. One approach to satisfy fully these key factors was to use the silicon carbide (SiC) grit-filled organic polymers as interior linings, which can be fabricated by centrifugal-casting technology. A polymer matrix that was found to bind the SiC grits, as the thermal conductor, into a coherent mass, was composed of a trimethylolpropane trimethacrylate (TMPTMA)-cross-linked styrene/methyl methacrylate polymer network. The thermal conductivity of SiC-filled polymer linings yielded by centrifuging it was 6.41 $W\,m^{-1}{}^{\circ}C^{-1}$, corresponding to about twice that of the bulk polymers without the SiC thermal conductors [1, 2]. Also, this value was very close to that of the high alloy stainless steel heat-exchanger tubes being used in geothermal power plants. Furthermore, this lining displayed an outstanding hydrothermal stability at 150 °C and protected the underlying MCS from corrosion.

Although the thermally conductive polymer-lined MCS tubes demonstrated their value as a heat exchanger, considerable attention had to be paid to the method of joining the tubes to the tubesheets. In terms of the rolled joint, the roller expansion process is among the most popular ways to make tube-to-tubesheet joints. Using this technology, MCS tubes undergo a 5%–6% reduction in wall thickness when they are rolled into a tubesheet [3]. Thus, one important concern about applying the coating materials to the interior surfaces of the bare tube ends is whether or not these coating systems can withstand a high compressive force and abrasive wear during the expansion process. The coating materials may be required to have specific properties, such as high plastic deformation to prevent the generation of any internal or

surface defects, and great surface hardness to confer resistance to abrasive wear. Unfortunately, the SiC-filled polymer linings were too brittle to withstand any type of expansion process. Even though the highly plastic polymer itself was applied as a coating, its lack of wear resistance caused the coating film to peel from the substrate's surfaces. Thus, finding a tough, ductile, wear/corrosion-resistant coating material to apply to $\sim 5$ cm of the interior end of the tube that is inserted in the tubesheet, is very important in extending the useful life-span of heat-exchanger tubes.

Nickel–aluminium (Ni–Al) coatings applied by the flame-spray coating technology are very attractive as a tube-end liner because they not only bond well to the metal surfaces, but also exhibit good plastic deformation, great wear resistance, a coefficient of thermal expansion similar to that of steels, and excellent thermal conductivity in the range 35–76 $W\,m^{-1}\,^{\circ}C^{-1}$ [4, 5]. Our preliminary estimate of the extent of deformation was obtained from a simple compressive expansion method simulating the roller expansion process; namely, a steel panel with an Ni–Al coating ($\sim 2$ mil thick; 1 mil $= 2.54 \times 10^{-5}$ m) was placed on a Carvel Laboratory Press having a maximum applied load of 10 800 kg, and then was compressed under 26.2 MPa loading. The reduction of coating thickness was $\sim 2.5\%$. No visual signs of the coating's failure such as lifting, delaminating, blemishes, or defects, were observed, verifying that the flame-sprayed Ni–Al materials possess good plastic deformation. However, the open porous structure that developed in the flame-sprayed coating layers was a critical issue in protecting the underlying steel substrates against corrosion. Hence, the use of sealing materials was required to fill these inherent openings.

Of particular interest was to apply the high-temperature performance polyphenylenesulphide (PPS) thermoplastic as the sealant on Ni–Al coating surfaces. The major characteristic of PPS, which is among the various polyaryl polymers, was the molecular orientation caused by chain extension at its melting point, $\sim 290\,^{\circ}C$. This orientation led to the formation of a semi-crystalline liner polymer during cooling. Such melt-crystallization behaviour of PPS gave it specific, desirable characteristics; it shows high-temperature hydrothermal stability, chemical resistance, and has excellent elongation properties [6].

From the information described above, emphasis in this present work was directed toward assessing the potential application of PPS as a sealant of the flame-sprayed Ni–Al coating. The research, therefore, focused on the two objectives: one was to investigate the changes in chemistry and microstructure of the Ni–Al coating itself without the sealants after exposure in the simulated geothermal environment; the second was placed on assessing the role of PPS sealant in improving the ability of Ni–Al coatings to reduce the rate of corrosion of the underlying steels. To achieve these goals, the coated MCS panels, after compression, were exposed to a corrosive solution consisting of 1.0 wt % $H_2SO_4$, 13.0 wt % NaCl, and 86.0 wt % water at 200 °C, under a hydrothermal pressure of 1.6 MPa. Then, the surfaces, subsurfaces, and interfaces of the coated panel specimens were explored to gain information on the changes in their chemical compositions and states, phase identification and transformation, morphological alterations, and interfacial bond structures. All the data were integrated and correlated directly with the results from the corrosion tests.

## 2. Experimental procedure

### 2.1. Materials

The metallic substrate used was a mild carbon steel (MCS). SW 3670 wires (ASB Industries, Inc. Orberton, OH) with a nickel/aluminium ratio of 80/20 by weight were used as the starting material for the Ni–Al coatings. The coatings were applied using a hand-held wire flame gun (Model 12E Perking–Elmer's Metco Westbury, NY) under an air pressure of $\sim 0.45$ MPa on to MCS specimens of 6.25 cm × 6.25 cm. Before spraying, the surfaces of MCS were cleaned and decontaminated by blasting them with silica grit with a particle size range 0.177–0.297 mm. The average depth of surface roughness of grit-blasted MCS, determined by a dektak surface profile measuring system (Sloan Technology Co., Santsa Barbara, CA), ranged from 0.02–0.045 mm. Once the wire reached its molten temperature in the propane flame, the molten Ni–Al particles were projected from a target distance of $\sim 10$ cm on to the MCS surfaces. At room temperature, the molten Ni–Al was completely converted into a solid coating within 1 min after spraying. The average thickness of this coating was $\sim 0.09$ mm. The X-ray diffraction analysis of this coating layer revealed that the major phase composition in the layers consisted of the two metal components, nickel and aluminium.

The PPS powder for the slurry coating was supplied by the Phillips 66 Company. The as-received PPS was a finely divided, tan-coloured powder having a high melt flow with a melting point of 288 °C. The PPS sealant was deposited on the Ni–Al-coated MCS panels in the following way. First, the coated panels were dipped into a PPS slurry consisting of 45 wt % PPS and 55 wt % isopropyl alcohol at 25 °C, and withdrawn slowly. The slurry-wetted panels were preheated in an air oven at 100 °C for 1 h to allow volatilization of the isopropyl alcohol liquid phase, and correspondingly to promote conversion of the slurry into the sintering layer. The sintered PPS layer was finally heated in air at 350 °C for 3 h to achieve its melt flow, and subsequently cooled to room temperature to fabricate a solid film. Cross-sectional examination using scanning electron microscopy showed that the thickness of the PPS sealant deposited on the Ni–Al coatings ranged from 0.01–0.05 mm. Finally, the PPS-sealed and unsealed Ni–Al coating panels were compressed under 26.2 MPa loading for 5 min. The resulting decreases in coating thickness were $\sim 3.1\%$ and $\sim 2.5\%$ for the sealed and unsealed coatings, respectively. The compressed test panels were exposed for up to 14 d in autoclave containing a low pH, hypersaline brine solution (1 wt % $H_2SO_4$, 13 wt % NaCl, and 86 wt % water) at 200 °C under a hydrothermal pressure of 1.6 MPa.

## 2.2. Measurements

A VG Scientific ESCA 3 MK II X-ray photoelectron spectrometer (XPS) was used to detect the chemical composition and states of the PPS-sealed and unsealed Ni–Al coating surfaces both before and after exposure to a harsh environment. XPS was also used to identify the locus of failure at the PPS/Ni–Al/MCS joints. The excitation radiation was provided by an $AlK_{\alpha}$ (1486.6 eV) X-ray source, operated at a constant power of 200 W and in a vacuum in the analyser chamber of $10^{-9}$ Torr (1 torr = 133.322 Pa). The atomic concentrations for the respective chemical elements were determined by comparing the XPS peak areas, which were obtained from differential cross-sections for core-level excitation. To set a scale in all the high-resolution XPS spectra, the binding peak was fixed at 285.0 eV as the internal reference. A curve-deconvolution technique, in conjunction with a DuPont curve resolver, was employed to find the individual chemical states from the high-resolution spectra of each element. To explore the morphological features and chemical profiles of the cross-sectional areas of PPS-sealed and unsealed Ni–Al coating specimens after autoclaving, pieces (10 mm × 10 mm) of the specimens were mounted in an epoxy resin and polished with an automatic polishing unit. Scanning electron microscopy (SEM, Model JXA-35, Jeol, Peabody, MA) coupled with energy-dispersive X-ray spectrometry (EDX, TN-5502, Tracor Northern, Madison, WI) gave us this information. A.c. electrochemical impedance spectroscopy (EIS) was used to evaluate the ability of the coating films to protect MCS from corrosion. The specimens were mounted in a holder, and then inserted into an electrochemical cell. Computer programs were prepared to calculate theoretical impedance spectra and to analyse the experimental data. Specimens with a surface area of 13 $cm^2$ were exposed to an aerated 0.5 N NaCl electrolyte at 25 °C, and single-sine technology with an input a.c. voltage of 10 mV (r.m.s) was used over a frequency range of 10 kHz to $10^{-2}$ Hz. To estimate the coating's protective performance, the pore resistance, $R_p$, was determined from the plateau in Bode-plot scans (impedance, (Ω cm) versus frequency (Hz) that occurred at low-frequency regions.

# 3. Results and discussion

## 3.1. Ni–Al coating

Before surveying insight into the chemical profile and microstructural view of the PPS-sealed Ni–Al coating panels, focus centred on investigating the changes in chemical composition and state, and on exploring the alteration of morphological features for the exposed Ni–Al coating itself. The fractions of the respective chemical elements were estimated by comparing the XPS Al 2p, Cl 2p, C 1s, O 1s, Fe 2p, Ni 2p, and Na 1s peak areas, which can be obtained from the differential cross-sections for core level excitation. All XPS measurements were made at an electron take-off angle of 40°, which corresponds to an electron-penetration depth of ~ 5.0 nm [7]; thus, the XPS data provide the atomic fractions present in the surface layers of an ~5.0 nm thick. Table I gives the XPS atomic fractions and ratios of the Ni–Al coating surfaces before and after exposure for up to 14 days. For unexposed Ni–Al coating panels, denoted as 0 day exposure time, the surface chemical composition included three major atoms, aluminium, carbon, and oxygen, with nickel as a minor one. The detected carbon may reflect surface contaminants. The other three atoms, aluminium, oxygen and nickel are likely to be associated with aluminium and nickel oxides. When the coating panels were exposed for 1 day in an autoclave, striking differences in a atomic fraction, compared with that of the unexposed ones, were as follows.

1. The concentrations of aluminimum and carbon atoms declined about 20% and 33% respectively, while more oxygen was incorporated into the surface layer.
2. A certain amount of new atoms, such as chlorine, iron and sodium was detected.
3. The concentration of Nickel doubled to 4.0%

Regarding Difference 2, considerable attention was paid to the emergence of the iron atom. Because the source of iron arises from the underlying steel, it is possible to assume that iron, together with an increasing oxygen content may be associated with the formation of iron oxides as the corrosion products of steel; meanwhile, both sodium and chlorine have migrated from the NaCl solution. This information strongly demonstrated that the Ni–Al coatings allow the corrosion fluid to permeate their layer easily under such pressure, thereby resulting in the corrosion of the underlying steel. Extending the exposure time to 3 day seemed to enhance the rate of corrosion because of an increased amount of iron from 1.7% to 2.5%. A further increase in its amount can be seen on the 14 days exposed panel surfaces. Correspondingly, the amount of oxygen increased with an extended exposure time. Another important aspect in the variation of atomic concentrations as a function of exposure time was the fact that the amount of aluminium which was one of the dominant atoms existing at the outer most surface

TABLE I Changes in atomic composition of Ni–Al coating surfaces as a function of exposure time

| Exposure time (days) | Atomic composition (%) | | | | | | | Atomic ratio | |
|---|---|---|---|---|---|---|---|---|---|
| | Al | Cl | C | O | Fe | Ni | Na | Fe/Al | Ni/Al |
| 0 | 27.5 | – | 39.4 | 31.0 | – | 2.1 | – | – | 0.1 |
| 1 | 22.0 | 4.3 | 26.4 | 41.1 | 1.7 | 4.0 | 0.5 | 0.1 | 0.2 |
| 3 | 19.9 | 6.2 | 23.1 | 43.7 | 2.5 | 4.0 | 0.6 | 0.1 | 0.2 |
| 14 | 17.4 | 9.9 | 20.8 | 44.2 | 2.7 | 4.3 | 0.7 | 0.2 | 0.3 |

site of the unexposed panel surfaces, tended to fall as autoclaving time was prolonged; contrarily, there was an increase in the amount of nickel. The atomic ratio of nickel to aluminium for the 14 day exposed panels was 0.3, corresponding to three times that of the unexposed ones.

To support this information, the high-resolution XPS Al 2p and Ni 2p3/2 core-level spectra for the unexposed and the 3 and 14 day exposed panels were inspected (Fig. 1). In the Al 2p region, the spectrum from the unexposed panel surfaces had two Gaussian peaks at the binding energy (BE) positions of 74.5 and 73.0 eV. The former peak, as the principal component, is ascribed to aluminium in the $Al_2O_3$, and the contributor to a shoulder peak at 73.0 eV can be assigned as aluminium in the aluminium metal [8]. A considerable decay of the peak excitation at 73.0 eV was observed from the 3 day exposed panels; meanwhile, the intensity of the peak at 74.5 eV had grown markedly. There was no significant difference in the spectral feature of the 14 day exposed panels. In the Ni 2p3/2 region, the spectral feature for the unexposed panels indicated the presence of two nickel compounds related to the peaks at 854.3 and 852.8 eV. The former peak, as the major component, perhaps originates from Nickel in the NiO, and the latter weak peak is due to the nickel in the nickel metal [9, 10]. Upon autoclave the panels for 3 and 14 days, the spectral features were converted into the excitation of a symmetrical signal peak from the asymmetrical one. The

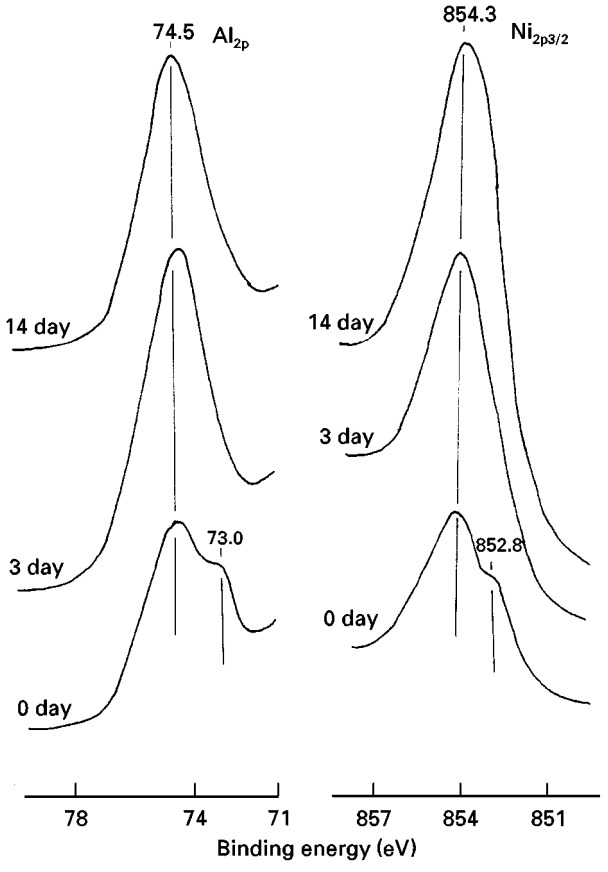


*Figure 1* XPS (a) Al 2p and (b) Ni 2p3/2 regions of Ni–Al coating surfaces before and after exposure for 3 and 14 days to hot brine solution at 200 °C.

spectra were characterized by the disappearance of the nickel metal peak at 852.8 eV, and the conspicuous growth of an NiO-associated peak at 854.3 eV. Relating this finding to the results from the previous atomic fractions, the integrated XPS examinations signified that the surface chemical states present in the top 5 nm layer of the unexposed Ni–Al coatings, are composed of the hybrid phases, $Al_2O_3$ and aluminium as the main components and NiO and nickel as the minor ones. Because two metal components, aluminium and nickel, arise from the bulk Ni–Al coatings, some of these surface components have already been oxidized during the flame-spraying process, forming $Al_2O_3$ and NiO. Once the Ni–Al coatings came into contact with a low-pH hypersaline brine solution at 200 °C, these metal components undergo oxidation, being converted into aluminium and nickel oxides. Hence, the hot brine solution at low pH acted as an oxidizing reagent of Ni–Al coatings.

As described in the surface atomic fraction study, aluminium was one of the dominant atoms occupying the top surface layer of the Ni–Al coatings, whereas nickel was the minor one. However, once the coatings were oxidized in this environment, the amounts of nickel and oxygen increased, while the amount of aluminium fell. This fact can be interpreted as follows; exposing the coatings to such an environment promoted the conversion of aluminium into the $Al_2O_3$ phase that serves as the primary barrier against oxidation of the coatings. Prolonged exposure times probably generate further $Al_2O_3$ growth, and also might cause the spallation of $Al_2O_3$ scales by creating a high stress at the Ni–Al metal/$Al_2O_3$ interfaces because of the difference in thermal expansion coefficients between the metals and oxide scales. After spalling, the underlying aluminium metal is again exposed and reoxidized to rebuild the oxidation protective $Al_2O_3$ scales. In other words, the consumption rate of aluminium from the coatings is inversely proportional to the thickness of $Al_2O_3$. Correspondingly, spalling of the $Al_2O_3$ scales eventually depletes aluminium, and subsequently, exposes nickel. Furthermore, the oxidation of nickel leads to the Ni → NiO phase transition. Nevertheless the Ni–Al coatings appear to suffer oxidation during their exposure to such an environment.

Because the exposed panel surfaces have some iron atoms, the Fe 2p3/2 core-level spectrum was also inspected to identify any iron related compounds. The surfaces of the 3 and 14 day exposed panel showed one resolvable component at 711.4 eV on overall excitation of the Fe 2p3/2 signal (not shown). According to the literature [11], the major contributor to this peak was judged to be iron in the $Fe_2O_3$ as the corrosion product of MCS. Consequently, although the repetitional processes of Al → $Al_2O_3$ → spallation, which can be visualized as a sacrificial mode, might protect the underlying MCS against the oxidation, the inherent porous structure in the Ni–Al coating layer caused the corrosion of MCS, allowing the corrosive brine to permeate its layers.

To visualize and substantiate these insights into the microstructure and chemical profiles of compressed Ni–Al coating layers before and after exposing them

for 14 days, the cross-sectional areas for the Ni–Al-coated steel panels were explored using SEM and EDX. Fig. 2 shows the SEM image and EDX spectrum of the unexposed Ni–Al panel. As is seen, although the coating was compressed under 26.2 MPa loading, the profile of Ni–Al layers revealed an interstitial porous microstructure. Attention then centred on the EDX tracings in the Ni–Al layers; it was found that the elemental composition of this layer depended on its different locations. The EDX spectrum at the upper site, denoted site "A", included the most intensive aluminium signal, a moderately developed nickel element, and a weak oxygen peak, demonstrating that the surface layers in the Ni–Al coatings had an aluminium-rich Ni–Al–O elemental distribution. The spectral feature of a middle location, such as site "B", had a markedly pronounced nickel signal, while the aluminium peak had become a secondary one, with a weaker oxygen peak. A further increase in the line intensity of nickel was observed at the critical interfacial boundary areas between the Ni–Al coating and MCS, denoted site "C". This spectrum also exhibited the presence of oxygen, although the intensity of its peak was very weak; it may have been introduced by the oxidation of the sprayed molten nickel and aluminium composites on to the MCS surfaces, and also due to the iron oxides existing at the outermost surface sites of MCS itself.

Fig. 3 shows the SEM surface image coupled with the EDX elemental analysis for 14 day exposed

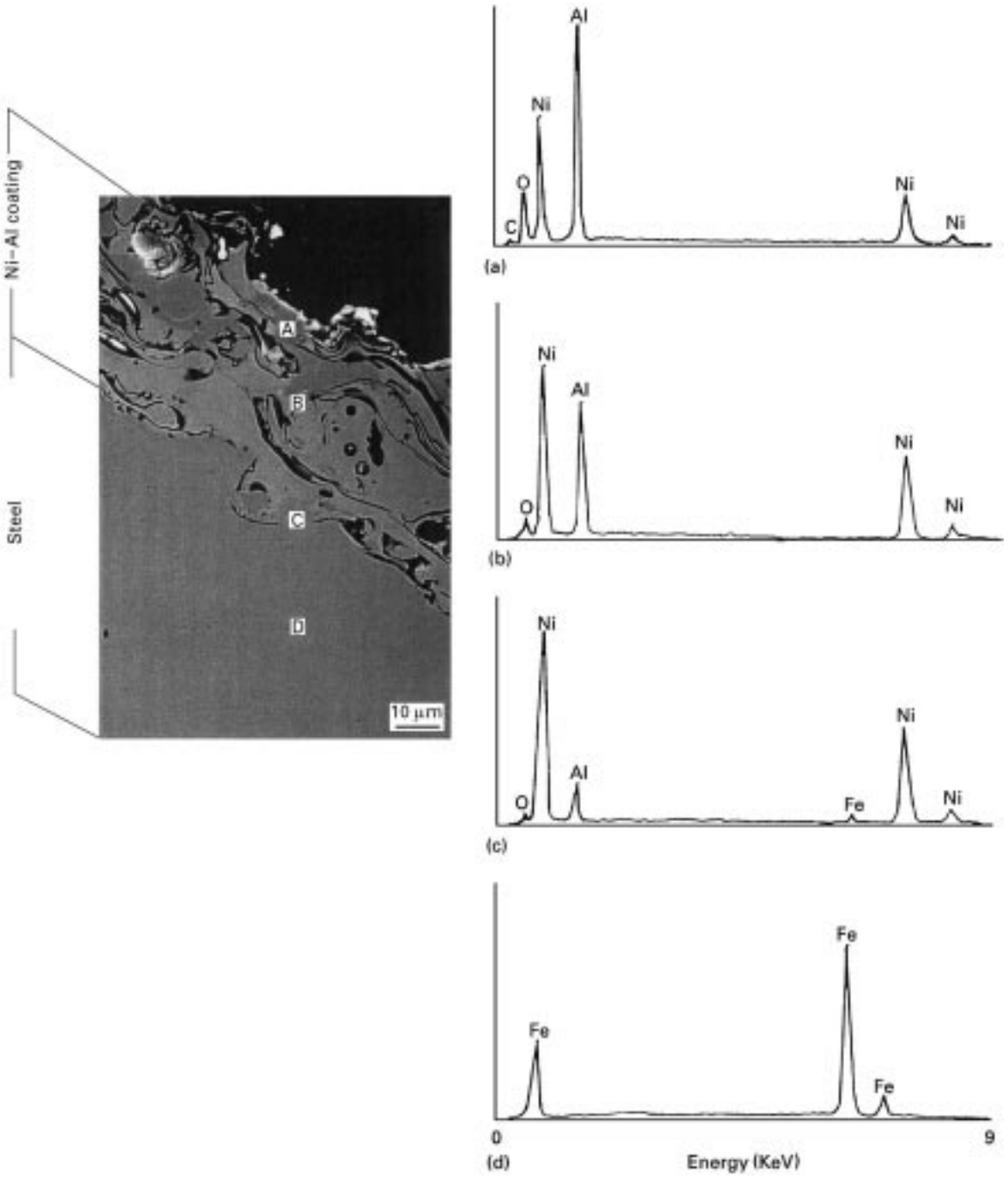


*Figure 2* (a) Scanning electron micrograph coupled with (b–e) EDX spectra for a cross-sectional area of the Ni–Al-coated steel panel before exposure. Areas: (b) A, (c) B, (d) C, (e) D.

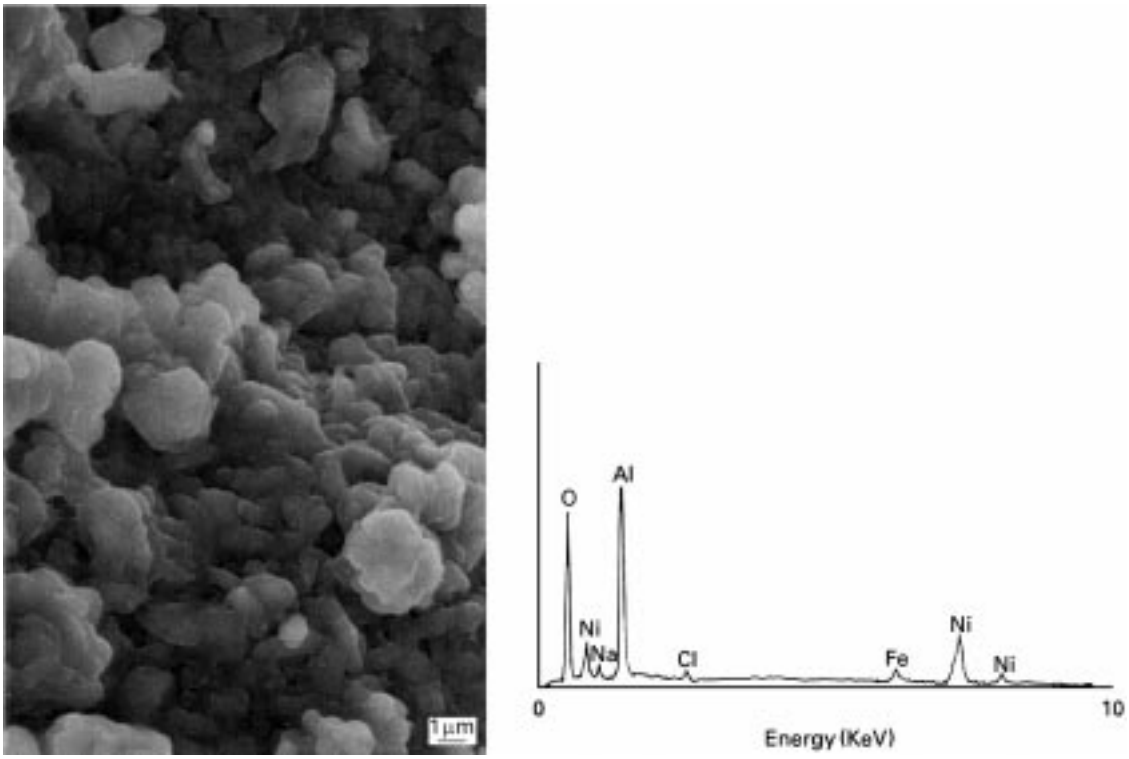


*Figure 3* (a) SEM image and (b) EDX spectrum for the surface of 14 days exposed Ni–Al coating.

samples. The morphological feature of the exposed Ni–Al coating surfaces was characterized by disclosing a continuous coverage of coalescent particles over the Ni–Al layers. The EDX spectrum for these particles had two strong peaks, aluminium and oxygen, seemingly reflecting the formation of $Al_2O_3$. This finding signified that the metallic aluminium component in the surface Ni–Al layers was preferentially oxidized by the geothermal fluid to form $Al_2O_3$, rather than nickel. As expected, the detection of an iron element related to an intense oxygen signal is ascribable to $Fe_2O_3$ as the corrosion product of the underlying steel. Both the sodium and chlorine in the spectrum come from the brine solution. By comparison with that of the unexposed samples (see Fig. 2), a striking difference in SEM image was observed in the cross-sectional area of the 14 day exposed samples (Fig. 4). There was a development of corrosion-generated stress cracks at the interfacial contact zone between the Ni–Al and steel. As is evident from EDX spectrum in the interfacial region, denoted site "B", this area had two strong signals, oxygen and iron, which are associated with the corrosion products of steel. In addition, the spectrum of location A at a distance of $\sim 10\,\mu m$ from the top surface of the Ni–Al layers included three conspicuous peaks, oxygen, aluminium and iron, together with a moderately grown nickel peak, demonstrating the $Fe_2O_3$ corrosion products had been transferred from the interfacial steel side to the Ni–Al layer. In other words, the open porous structure of the Ni–Al coating allowed a hot brine solution to infiltrate, which then led to an increase in the rate of corrosion of the steel, thereby resulting in the development of the interfacial stress cracks caused by the growth of $Fe_2O_3$-related corrosion products at interfaces. This information strongly demonstrated that the use of a sealing material on the outer coating surfaces is needed to prevent the penetration of corrosive species through the coating.

## 3.2. PPS sealant

Fig. 5 represents the SEM image of the PPS-sealed Ni–Al coating surfaces after exposure for 14 days, showing the rough surface microtexture of the sealant covering the coating surfaces. The EDX spectrum concomitant with the SEM, included a strong sulphur signal and four minor peaks, carbon, oxygen, sodium and chlorine. The contributors to the sulphur and carbon elements, and to the sodium and chlorine ones, conceivably are the PPS and the brine solution, respectively. One important concern about the presence of oxygen was whether or not its incorporation into the surface layers is due to the oxidation of PPS. To resolve this question, XPS analysis for the unexposed, and the 3 and 14 day exposed PPS/Ni–Al coating surfaces was conducted to gain information on the degree of PPS oxidation as function of exposure time. Table II gives the changes in its chemical composition and in the atomic ratios of C/S and O/C for the specimens before and after exposure. The amount of oxygen increases with longer exposure time; contrarily, there was a decrease in amounts of both the sulphur and carbon atoms arising from PPS. Correspondingly, the O/S and O/C ratio was raised as exposure time was prolonged, suggesting that exposing the PPS to such an environment leads to the incorporation of more oxygen into its surface layer. In other words, PPS can undergo oxidation during exposure to a hot brine solution at 200 °C.

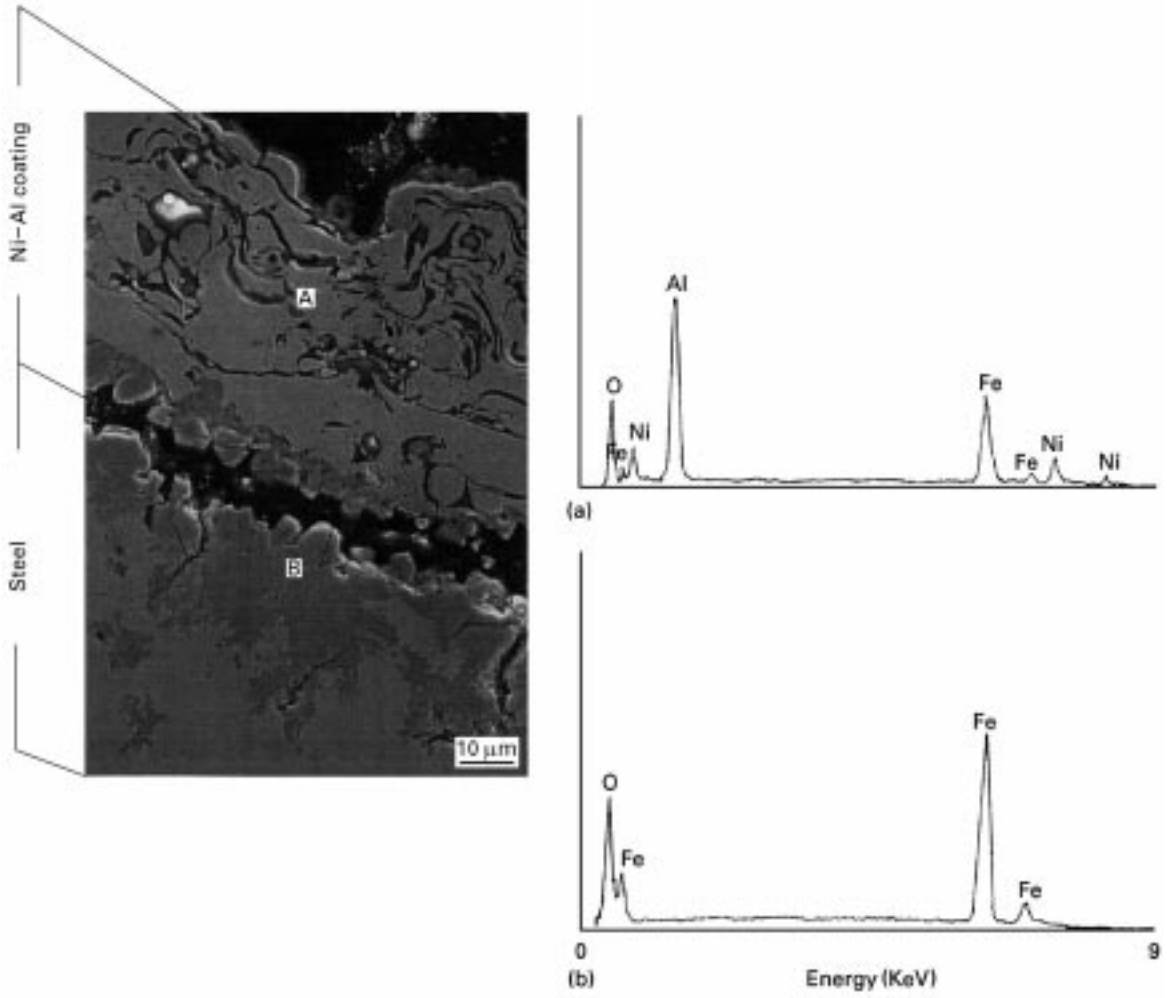


*Figure 4* SEM–EDX analyses of a cross-sectional area in the Ni–Al/steel joint system after exposure for 14 days. (a) Scanning electron micrograph, (b,c) EDX for areas (b) A, and (c) B.

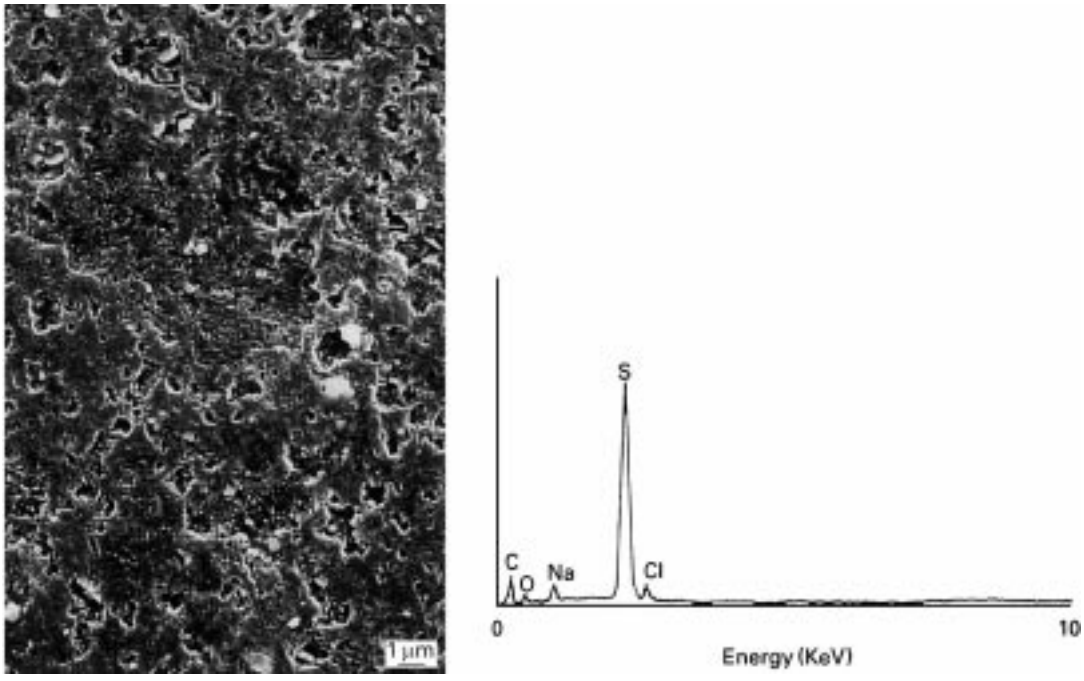


*Figure 5* (a) SEM image concomitant with (b) the EDX spectrum for the 14 days exposed PPS coating surfaces.

TABLE II Changes in atomic fraction and ratios of PPS surface as a function of exposure time

| Exposure time (days) | Atomic fraction (%) | | | | | Atomic ratio | |
|---|---|---|---|---|---|---|---|
| | S | Cl | C | O | Na | O/S | O/C |
| 0 | 13.0 | – | 81.6 | 5.4 | – | 0.4 | 0.1 |
| 3 | 8.0 | – | 68.0 | 24.0 | – | 3.0 | 0.4 |
| 14 | 4.2 | 1.7 | 64.2 | 28.6 | 1.3 | 6.8 | 0.5 |

Next, focus centred on identifying the reaction products yielded by oxidation of PPS. The XPS S 2p region for the unexposed and exposed specimens surfaces was inspected to gain this information (Fig. 6). The overall spectra of the unexposed specimens, marked as 0 days, indicated the excitation of a symmetrical single peak at 163.8 eV, representing sulphur in the PPS [12]. Of particular interest was the spectrum excited from the 3 day-exposed one. As shown, in S 2p region had an additional signal at 167.7 eV, corresponding to a shift in the high BE site of 3.9 eV above that of sulphide-related peak in the PPS as the principal component at 163.8 eV. An XPS study on sulphur–oxygen bonds [13, 14] suggested that the increase in the rate of oxidation of sulphur results in a shift in peak position to a high BE site; for instance, sulphoxide ($>S=O$) around 165.9 eV, sulphone ($>SO_2-$) at $\sim$ 167.5 eV, and sulphate ($-SO_4$) at $\sim$169.0 eV. From this information, it can be assumed that the contributor at 167.7 eV is attributable to the formation of polysulphone, $-[-SO_2-]-_n$, transformed by the oxidation of sulphide groups within the PPS. Such sulphide-sulphone transformation seems to take place during the 3 day exposure to hot brine. A further increase in the degree of oxidation for the 14 day specimens involved another additional peak at 169.2 eV in the S 2p region, forming a different sulphur–oxygen product from the sulphide- and sulphone-based compounds. This signal, which emerged at a higher BE site, can be ascribed to the sulphur originating from the sulphate. Turner *et al.* [15] reported that the peak excitation originating from the sulphur in sodium sulphate, $Na_2SO_4$, occurs near 169.0 eV. Assuming that the contributor to this peak is the sulphate-related compounds, the enhanced oxidation of polyphenylsulphone may cause its decomposition to form a sodium sulphate derivative. Although there is no clear evidence about its derivation, the following hypothetical oxidation pathway of the PPS may account for these observed changes

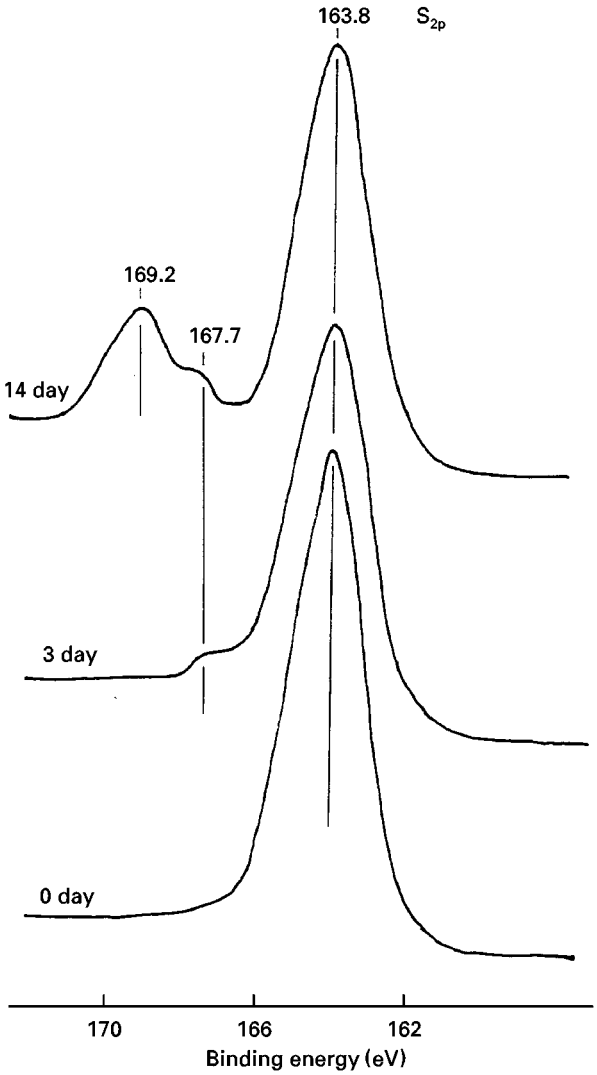


*Figure 6* S 2p region for the unexposed, and the 3 and 14 days exposed PPS surfaces.

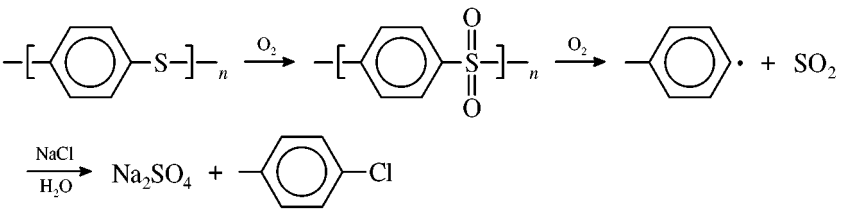


(1)

First, the sulphide → sulphone conformational change may take place in the oxidized PPS structure. A second oxidation process is the decomposition of the polyphenylsulphone, which yields two derivatives, aryl radical and $SO_2$ gas. Finally, the interaction between the $SO_2$ and the $Na^+$ dissociated from NaCl in an aqueous medium provided the formation of sodium sulphate; meanwhile, the $Cl^-$ ion as a counter

ion of $Na^+$ may react with the aryl group having a free radical. This reaction may result in the formation of polychloroaryl compounds [16, 17]. Again, the XPS Cl 2p core-level spectrum of the 14 day-exposed specimens was investigated to ascertain whether or not the chloroaryl group actually yields in an exceedingly oxidized PPS conformation. The spectrum (not shown) verified that this group forms in the oxidized PPS because of the excitation of a marked peak at 201.3 eV, originating from chlorine in the chlorobenzene compounds [18]. Considering the high solubility of the sodium sulphate compound in water, its dissolution in an aqueous medium might cause the hydrolysis of PPS. Hence, this finding can be taken as evidence that the PPS is susceptible to oxidation reaction with a hot brine solution. However, no study was made on the kinetics of this reaction, so we cannot predict how long the PPS sealant can withstand such a harsh environment.

Nevertheless, Fig. 7 represents the results from the SEM-EDX analysis of the cross-sectional profile for the PPS-sealed Ni–Al coatings after exposure for 14 days. There was a marked difference in this SEM image from that of the unsealed Ni–Al coating specimens (see Fig. 4); namely, there was no clear evidence of developing microcracks caused by the corrosion of the underlying steels at the critical interfacial contact zones between the Ni–Al coating and steel, marked site "C". The EDX spectrum (C) supported this fact; it exhibited a very weak signal of oxygen, together with

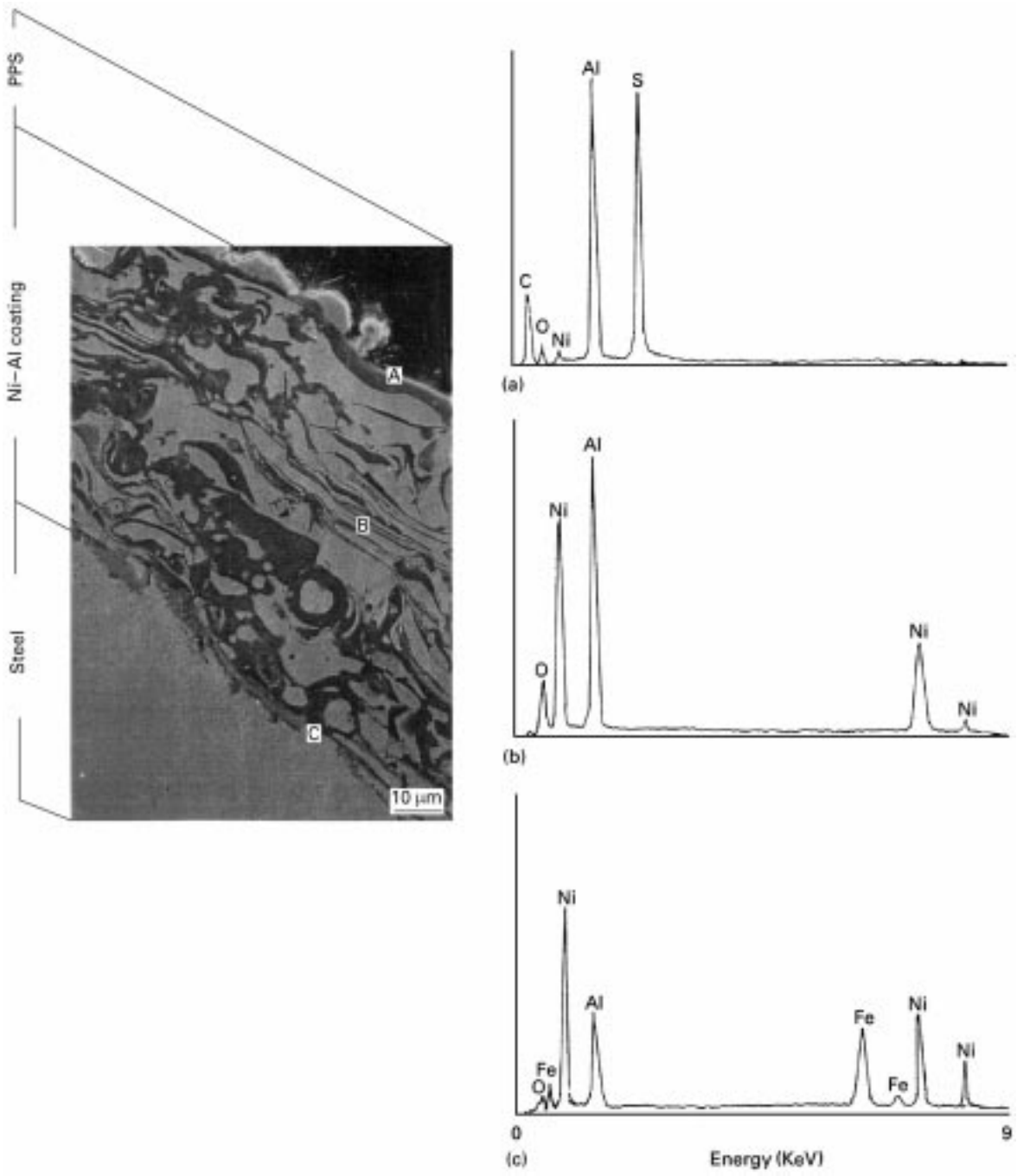


*Figure 7* SEM–EDX analysis for a cross-sectional profile in the 14 days exposed PPS/Ni–Al/steel joint system. (a) Scanning electron micrograph, (b) EDX of area A, (c) EDX of area B, (d) EDX of area C.

the strong nickel related peaks, and the moderately grown aluminium and iron peaks. For more information, the feature of the EDX spectrum taken from the interfacial PPS/Ni–Al regions, denoted site "A", seems to demonstrate that the sulphur in the PPS preferentially reacts with the aluminium in the Ni–Al coatings, rather than nickel because of the presence of two prominent peaks, the aluminium and sulphur elements. The carbon element belonging to the PPS showed a moderate intensity in conjunction with a lesser oxygen and nickel signal, suggesting that although the PPS suffered oxidation damage from the hot brine, the degree of oxidation at the interfacial PPS/Ni–Al regions was very little, if any. As a result, a PPS sealant, with 0.01–0.05 mm thick, significantly served in reducing the degree of oxidation for both the Ni–Al coating and the underlying steel exposure for 14 days to a hot brine solution at 200 °C.

Next, attention was directed to visualizing how well the PPS sealant adheres to the Ni–Al coating, and also to identify any possible reaction products and bond structures formed at the interfaces between the PPS and Ni–Al before and after 14 days. Again, XPS was used to inspect both the interfacial PPS and Ni–Al sites of PPS-sealed Ni–Al coating specimens that had been physically disrupted by a tensile force. Table III gives the atomic fractions of the PPS and Ni–Al interfaces for the unexposed and exposed specimens. For the unexposed PPS/Ni–Al joint specimens, the interfacial PPS side separated from the Ni–Al coating had 28.0% Al and 1.6% Ni. Because these atoms arise from the Ni–Al coating, this finding follows that a certain amount of Ni–Al transfer to the PPS side during the failure of interfacial bonds. The atomic fraction from the interfacial Ni–Al site closely resembled that of the PPS interfaces, indicating that the loss of interfacial adhesion occurred in the mixed layers of PPS and Ni–Al, reflecting a good adherence of the PPS sealant to the Ni–Al coating. In contrast, when this joint specimen was exposed for 14 days in a hot brine solution, more oxygen was incorporated and inserted into the interfacial regions. In fact, an oxygen content of $> 40\%$ was detected at both interfacial sites, while the amount of carbon was markedly reduced. The data also showed that the locus of bond failure was similar to that of the unexposed specimens; the disbondment took place in the PPS/Ni–Al mixed layers. Consequently, the focus centered on answering one important question: what is the role of PPS sealant in improving the adherence to the Ni–Al coating? In response to this question, the reaction products yielded at the interfaces between the PPS and Ni–Al layers were identified by inspecting XPS Al 2p and Ni 2p3/2 core-level spectra for the specimens on the interfacial Ni–Al side removed from the PPS sealant before and after exposure.

TABLE III Chemical composition (wt %) of both interfacial failure sides for PPS/Ni-Al joint specimens before and after exposure for 14 days in an Autoclave at 200 °C

| | | wt % | | | | |
|---|---|---|---|---|---|---|
| Exposure | Side | Al | S | C | O | Ni |
| Before | PPS | 28.0 | 4.4 | 37.5 | 28.5 | 1.6 |
| Before | Ni–Al | 26.6 | 4.2 | 35.7 | 32.0 | 1.6 |
| After | PPS | 28.1 | 3.8 | 23.7 | 42.1 | 2.3 |
| After | Ni–Al | 25.6 | 3.1 | 22.7 | 46.1 | 2.5 |

In the Al 2p region (Fig. 8), both the unexposed and exposed specimens showed the excitation of a single peak at 76.3 eV; meanwhile, there were no peak excitations at 74.5 and 73.0 eV, belonging to the aluminium in the $Al_2O_3$ and in the metallic aluminium, respectively. Our earlier work on investigating the interface of PPS-to-steel joints prepared in air or nitrogen at 350 °C, demonstrated that the oxidation of PPS in air at high temperatures led to the evolution of $SO_2$ gases, thereby resulting in the introduction of sulphur-associated reaction products, such as $Fe_2(SO_4)_3$, $FeSO_4$, and FeS, into the critical interfacial boundary zones [19]. It can be expected that this new signal at 76.3 eV is due to the interfacial reaction products formed by interaction between the $Al_2O_3$ in Ni–Al and the $SO_2$ gas evolved from PPS. To identify this Al–S-related reaction product, two reference compounds, the aluminium sulphate $[Al_2(SO_4)_3]$ and aluminium sulphide ($Al_2S_3$) were examined. The peak positions from the Al 2p spectrum of these reference compounds were 76.0 and 74.9 eV for $Al_2(SO_4)_3$ and $Al_2S_3$, respectively. The major contributor to this new peak, therefore, was assigned as aluminium in the $Al_2(SO_4)_3$, which formed as the interfacial reaction product. However, there is no evidence as to whether the reaction between $Al_2O_3$ and $SO_2$ to form $Al_2(SO_4)_3$ takes place in a direct or indirect manner. Nevertheless, this reaction product appears to be yielded at the interfaces of the joint specimens before exposure. Relating this finding to the incorporation of more oxygen into the interfacial zones after exposure, there is no doubt that the increase in the degree of PPS oxidation as a function of

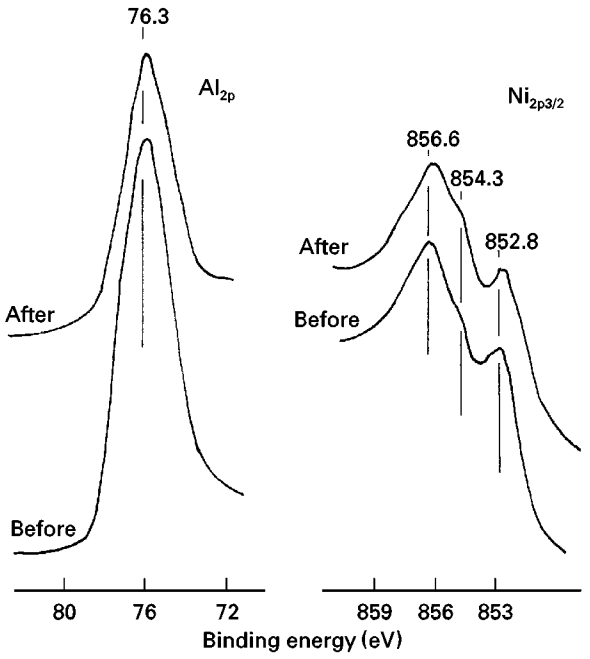


*Figure 8* (a) Al 2p and (b) Ni 2p3/2regions on interfacial Ni–Al sides removed from PPS in PPS-sealed Ni–Al coating system before and after exposure for 14 days.

exposure time corresponds to an enhancement in the emission of $SO_2$, so increasing the amount of $Al_2(SO_4)_3$. The survey of Ni 2p3/2 core-level excitation (Fig. 8) indicated the presence of three resolvable peaks at 856.6, 854.3, and 852.8 eV. According to the literature [9, 10, 20], the first peak as the principal component is likely to be associated with nickel in the $NiSO_4$ and the second and third peaks as minor ones reveal the nickel in the NiO and metallic nickel, respectively. From this result, the $SO_2$ not only reacts with the $Al_2O_3$ to form $Al_2(SO_4)_3$ but also has some chemical affinity for NiO. Such chemical attraction might lead to the formation of the $NiSO_4$ reaction product. From the evidence that the amount of aluminium at the locus of the bond failure was considerable higher than that of nickel for both the unexposed and exposed specimens (see Table III), the quantity of this interaction product would be very small, compared with that of $Al_2(SO_4)_3$, due to the preferential uptake of $SO_2$ by $Al_2O_3$ rather than by NiO.

### 3.3. Corrosion resistance

Although the $Al_2(SO_4)_3$ salt, as the major reaction product, plays an essential role in improving the interfacial bond, there remains a question that must be answered in the affirmative; namely, does this water-soluble reaction product serve in inhibiting the corrosion of the underlying steel? Furthermore, once PPS has been oxidized by hot brine, how extensive is its efficacy and ability to prevent permeation of the corrosive ions through the sealing layer? To answer these questions, emphasis focused on investigating the magnitude of ionic conductivity generated by the electrolyte passing through the PPS-sealed Ni–Al coating layers. An electrochemical impedance spectroscopy (EIS) test was conducted on the unsealed and sealed coating specimens as a function of exposure times up to 14 days. Fig. 9 gives the Bode-plot features (the absolute value of impedance $|Z|$, versus frequency, of the unexposed specimens. Particular attention in the overall impedance curve was paid to the impedance value, called the pore resistance, $R_p$, which can be determined from the plateau in the Bode-plot occurring at sufficiently low frequencies [21]. A high value of $R_p$ results in a low degree of penetration of electrolyte into the coating layer, corresponding to an impervious coating layer.

As is seen, the $R_p$ value of the Ni–Al coating at 0.01 Hz was $\sim 8.0 \times 10^2$ of $cm^2$. When the coating was sealed with the PPS, its value increased by nine orders of magnitude over that of the unsealed one. Thus, the unexposed PPS sealant appears to minimize greatly the rate of penetration of NaCl electrolytes into the coating layers, conferring resistance to the corrosion of underlying steel. Fig. 10 depicts the changes in $R_p$ at 0.01 Hz for these specimens; there was a gradual reduction in the $R_p$ value for the PPS-sealed Ni–Al coating specimens during exposure of up to 14 days. Hence, prolonged exposure led to the uptake of more electrolytes by the PPS sealant, thereby poorly protecting the underlying steel against corrosion. There are two reasons for such uptake: one is the decline in the efficacy of the sealing layers caused by the susceptibility of PPS to oxidation reaction with a hot brine, and the other may be due to the increase in the amount of water-soluble $Al_2(SO_4)_3$ salt yielded by the interaction between the $SO_2$ evolved from the excessively oxidized PPS sealant and the $Al_2O_3$ in the Ni–Al coating during exposure. For the latter aspect, the formation of $Al_2(SO_4)_3$ salt in the interfacial transition zones between the PPS and Ni–Al layers may be

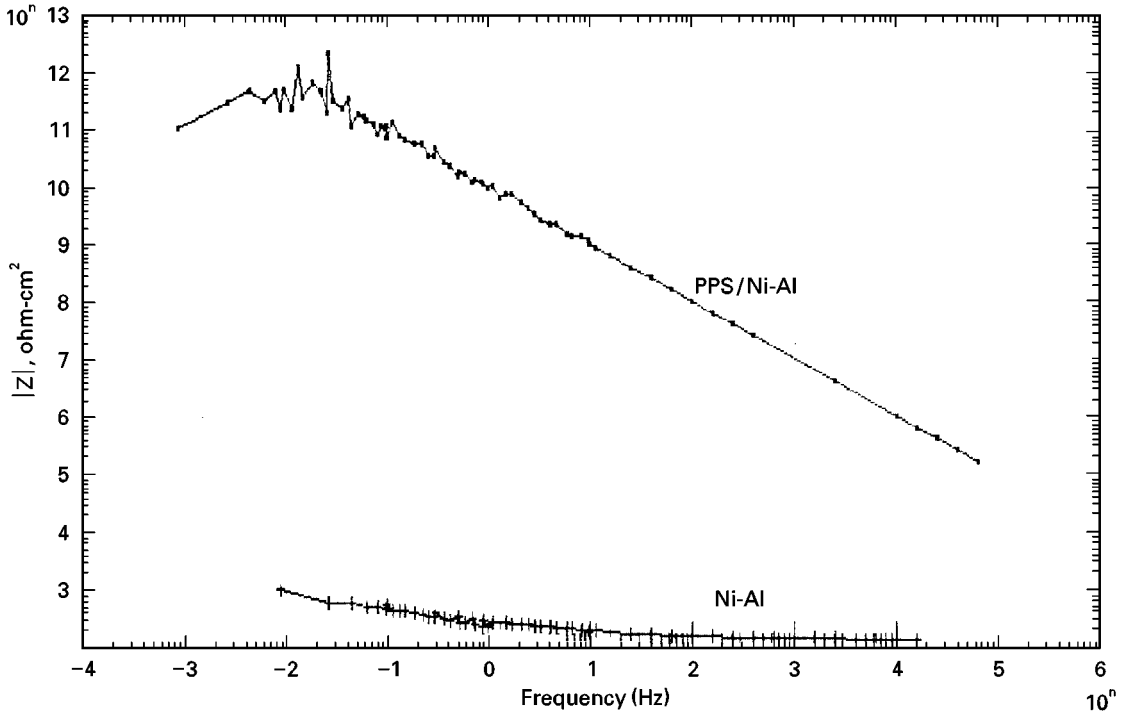


*Figure 9* Bode-plots for PPS-sealed and unsealed Ni–Al coating panels.

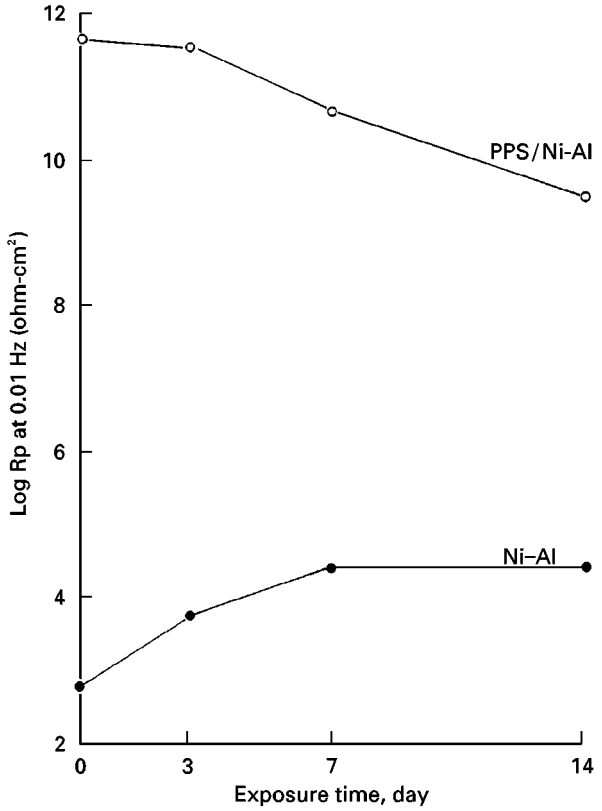


*Figure 10* Changes in $R_p$ at 0.01 Hz for PPS-sealed and unsealed Ni–Al coatings as a function of exposure time.

critical in reducing the rate of permeation of corrosive electrolytes in the Ni–Al layers because of its high solubility in water.

By comparison, the unsealed Ni–Al coatings showed that the $R_p$ value tends to increase slightly with prolonged exposure time before leveling off for a period of 7 days. Because the increase in $R_p$ is responsible for lowering of its ionic conductivity, this fact is taken as evidence that the top surface layers of Ni–Al coating became a densified and insulated structure. Such structural alteration perhaps reflects the growth of $Al_2O_3$ scale arising from the oxidation of Ni–Al coating surfaces (see Fig. 3); a continuous coverage of coalescent $Al_2O_3$ scales over the Ni–Al coating might develop into a dense, insulating surface structure that minimizes the permeation of ionic species.

## 4. Conclusion

The following conclusions can be drawn from these assessments of the usefulness of polyphenylenesulphide (PPS)-sealed Ni–Al coatings in protecting the interior surfaces at the ends where the bare heat-exchanger tube is jointed to a tubesheet by the roller expansion process, from the corrosion, oxidation, and abrasive wear in a low-pH hypersaline geothermal environment at 200 °C under hydrothermal pressure of 1.6 MPa. Although the flame-sprayed Ni–Al coating were compressed under a 26.2 MPa loading to simulate the roller expansion process, the inherent open pores and void spaces present in the coating layers were a critical issue in protecting the underlying steel substrates against corrosion, allowing the corrosive ionic species to permeate the coating layer. In fact, unsealed Ni–Al coating panels after exposure for 14 days to a hot brine solution (1.0 wt % $H_2SO_4$, 13 wt % NaCl and 86.0 wt % water) at 200 °C developed corrosion-generated stress cracks at the interfacial contact zone between the Ni–Al and steel. In addition, the coating suffered oxidation during exposure, leading to the growth of $Al_2O_3$ as the major scale compound, and NiO as the minor one. In attempting to improve its resistance to corrosion and oxidation, the surface of the Ni–Al coating was sealed with thermoplastic PPS.

One drawback of PPS was its susceptibility to oxidation reaction with a hot brine. This reaction, initiated by sulphide-sulphone transformation within the PPS, caused the decomposition of PPS to form a polychoroaryl compound and sodium sulphate salt, and the evolution of $SO_2$ gases. The $SO_2$ gases favourably reacted with the oxide compounds of Ni–Al coating to yield $Al_2(SO_4)_3$ as the principal reaction product and $NiSO_4$ as the minor one at the critical interfacial boundary region between PPS and Ni–Al layers. Although these reaction products offered improved adherence of PPS to Ni–Al, their solubility in water created unstable intermediate layers. These undesirable factors promoted the uptake of corrosive electrolytes by PPS during prolonged exposures. However, there was no development of corrosion-induced cracks at the interfaces between the underlying steel and the Ni–Al coating, nor was there striking oxidation of the sealed coating panels after exposure for 14 days. These findings suggested that PPS sealant improves the corrosion- and oxidation-resistance of the Ni–Al coating during a short-term exposure.

## Acknowledgement

This work was performed under the auspices of the US Department of Energy Washington, DC, under contract DE-AC02-76CH00016.

## References

1. J. J. FONTANA, W. REAM and H. C. CHENG, In "5th International Congress on Polymer in Concrete", edited by B. W. Staynes (Brighton Polytechnic, Brighton, 1987) p. 399.
2. V. HASSANI and E. HOO,"Results of Field Testing on Heat Exchangers with Polymer Concrete lining", National Renewable Energy Laboratory (NREL) USA (1995).
3. M. KINDSCHI, personal communications, Hughes-Anderson Heat Exchangers, Inc. July (1997).
4. S. SAMPATH, G. A. BANKE, H. HERMAN and S. RANGASWAMY, *Surf. Eng.* **5** (1989) 293.
5. D. N. RONALD, R. B. RANDY and M. V. NATHAL,"Physical and Mechanical Metallurgy of NiAl", National Aeronautics and Space Administration (NASA) Technical Paper 3398, April (1994).
6. M. S. REISCH, *Chem. Eng. News* **71** (1993) 24.
7. M. P. SEAH and W. A. DENCH, *Surf. Interface Anal.* **1** (1979) 2.
8. D. E. PASSOJA, H. F. HILLERY, T. G. KINISKY, H. A. SIX, W. T. JANSEN and J. A. TAYLOR, *J. Vac. Sci. Technol.* **21** (1982) 933.

9. K. S. KIM and R. E. DAVIS, *J. Electron Spectrosc.* **1** (1973) 251.
10. E. W. A. YOUND, J. C. RIVIERE and L. S. WELCH, *Appl. Surface Sci.* **28** (1987) 71.
11. N. S. McINTYRE and D. G. ZETARUK, *Anal. Chem.* **49** (1977) 1521.
12. J. RIGA, J. P. BOUTIQUE, J. J. VERBIST, In "Physicochemical Aspects of Polymer Surfaces", edited by K. L. Mittal (Plenum Press, New York, 1983) p. 45.
13. B. J. LINDBERG, K. HAMRIN, G. JOHNASSON, U. GELIUS, A. FAHLMAN, C. NORDLING and K. SIEGBAHN, *Phys. Scripta* **1** (1970) 286.
14. C. E. MIXAN and J. B. LAWBERT, *J. Org. Chem.* **38** (1975) 1350.
15. N. H. TURNER, J. S. MURDAY and D. E. RAMAKER, *Anal. Chem.* **52** (1980) 84.
16. R. W. LENZ and W. K. CARRINGTON, *J. Polym. Sci.* **41** (1959) 333.
17. *Idem*, *ibid.* **43** (1960) 167.
18. D. T. CLARK, D. KILCAST, W. K. R. MUSGRAVE, *J. Chem. Soc. Chem. Commun.* **4** (1971) 517.
19. T. SUGAMA and N. R. CARCIELLO, *J. Adhes. Adhesive* **11** (1997) 97.
20. R. B. SHALVOY and P. J. REUCROFT, *J. Vac. Sci. Technol.* **16** (1979) 567.
21. F. MANSFELD, M. N. KENDIG and S. TSAI, *Corrosion* **38** (1982) 570.

*Received 30 October 1997*
*and accepted 15 May 1998*